metals

MDPI

Article

Effect of Different Heat Treatments on Tensile Properties and Unnotched and Notched Fatigue Strength of Cold Work Tool Steel Produced by Powder Metallurgy

Alessandro Morri [1,*], Lorella Ceschini [1] and Simone Messieri [2]

[1] Department of Industrial Engineering (DIN), Alma Mater Studiorum, University of Bologna, Viale Risorgimento 4, 40136 Bologna, Italy; lorella.ceschini@unibo.it
[2] Ducati Motor Holding, Via Cavalieri Ducati Antonio 3, 40132 Bologna, Italy; simone.messieri@ducati.com
* Correspondence: alessandro.morri4@unibo.it; Tel.: +39-0512093463

Abstract: The present study investigates the effect of two heat treatments on the microstructure, the tensile and the fatigue properties of a powder metallurgy tool steel that has undergone two heat treatments: quenching and multiple tempering (conventional for powder metallurgy tool steel), and quenching and multiple tempering with an intermediate cryogenic step at −80 °C (new solution). The findings of the research indicated that the new heat treatment promotes the development of a homogeneous distribution of carbides in the martensitic matrix, with an increase of about 10% in tensile strength and about 7% in elongation to failure. This combination of exceptional strength with a high degree of toughness leads to an improvement in the fatigue behaviour of the steel, which exhibits a higher unnotched and notched fatigue strength (about 15% and 25% respectively) and a lower fatigue notch factor (about 15%) compared to conventionally heat-treated steel. These results highlight that the powder metallurgy tool steel, with the new heat treatment, could be a viable option for the production not only of tools and dies, but also for high-performance automotive components, including even those with complex geometries, such as camshafts or crankshafts.

Keywords: tool steels; powder metallurgy; heat treatment; microstructure; tensile strength; fatigue; nanoindentation

Citation: Morri, A.; Ceschini, L.; Messieri, S. Effect of Different Heat Treatments on Tensile Properties and Unnotched and Notched Fatigue Strength of Cold Work Tool Steel Produced by Powder Metallurgy. *Metals* **2022**, *12*, 900. https://doi.org/10.3390/met12060900

Academic Editor: Hana Jirková

Received: 27 April 2022
Accepted: 21 May 2022
Published: 25 May 2022

1. Introduction

The need to reduce polluting emissions is forcing designers of vehicles to lighten the chassis and also to downsize the engines. This requires the mechanical components to operate at their strength limits, resulting in higher requirements for the materials used. In order to meet this need, new steels produced by ESR (Electro-Slag Remelting) or VAR (Vacuum Arc Remelting) are increasingly being used in the transport field, because of their cleanliness, controlled microstructure and high performance. Recently, the steel producers, such as Böhler Edelstahl Gmbh [1] and Erasteel [2] have developed a new generation of "ultra-clean" powder metallurgy (PM) tool steels, also suitable for replacing nitriding or nitrocarburising steels in high performance automotive and motorcycle components due to their mechanical and microstructural features [3,4]. PM tool steels are generally produced via hot isostatic pressing (HIP) of powders obtained by inert gas or water atomization of molten steel [5]. HIP generally results in full-dense, porosity-free parts with uniform, equiaxed microstructure [6]. The current generation of gas atomization technology guarantees the production of fine and homogeneous powders with a mean particles size of approximatively 60 µm and a maximum size not exceeding 500 µm. The small size of the powders (about half compared to traditional PM process) combined with the strictly controlled composition reduces the segregations, the amount and size of non-metallic inclusions, the presence of large carbides or carbides clusters and porosity in the final product after HIP.

It is known that, in tool steels, non-metallic inclusions, large carbides and carbide clusters reduce steel toughness and generally act as fatigue crack nucleation sites, as extensively described in the published literature [3,7–17]. Therefore, the reduction of both quantity and size of non-metallic inclusions and alloying carbides, as well as the improvements of carbide distribution, can lead to a significant improvement in mechanical performance, making tool steels attractive candidates for critical components in automotive and motorsport applications.

However, in order to fully exploit the potentiality of ultra-clean PM tool steels and to enhance steel performance and/or to adjust its properties for specific applications, it is essential to optimize the heat treatment conditions [3,18]. Traditionally, tool steels undergo a quenching and multiple tempering heat treatment to obtain a tempered martensite microstructure with a uniform distribution of alloying carbides, which gives appropriate hardness and wear resistance. Several works [19–22] highlighted the importance of choosing the proper austenitizing and tempering temperatures. The first mainly controls: (i) the dissolution of primary carbides, thus influencing their amount and size after quenching; (ii) the amount of carbon and alloying elements in the austenite, and consequently the mechanical properties of the martensite and the amount of retained austenite after quenching. The latter influences the properties of tempered martensite, the amount of retained austenite after tempering and the precipitation of secondary alloying carbides. Broadly speaking, a low austenitizing temperature combined with a high tempering temperature improves fracture toughness and elongation to failure, but also decreases hardness. The opposite combination, high austenitizing and low tempering temperatures, improves hardness and wear behaviour but reduces ductility and toughness.

In most demanding automotive, aerospace and manufacturing applications, steel often also undergoes a cryogenic treatment (CT) [22–36] which provides a sound combination of hardness, wear resistance, toughness and deformation work [22–25,28–30]. Moreover, it is widely accepted that the addition of a cryogenic step to the heat treatment also leads to an overall increase in fatigue strength [18,27,31,32], although few experimental data are available on the fatigue behaviour of notched components [30–32]. Vahdat et al. [31] has shown that cryogenic treatment between quenching and tempering improves fatigue strength and tensile strength, but decreases impact strength of the 45WCrV7 tool steel. Shinde et al. [32] concluded that the fatigue strength of cryogenically treated AISI H13 die steel is improved compared to conventionally hardened and tempered steel. Niaki et al. [30] pointed out that cryogenic treatment after quenching does not alter the notch fatigue strength of the 1.2542 tool steel, but reduces the scatter of fatigue data.

At sub-zero temperatures, the strain energy and instability of martensite increase, thus forcing the carbon atoms to relocate and cluster to dislocation sites. These sites act as nuclei for the precipitation of nanometric secondary carbides, thus increasing toughness and blocking the propagation of cracks [22,24,28–30]. The greatest properties are obtained by carrying out CT after quenching and before tempering even if treating the steel at the end of the usual heat treatment cycle can also result in significant improvement Pellizzari, Molinari and Sola [23,25,35]. However, to take full advantage of the CT, it is important to bear in mind that its effect also depends on steel composition, austenitizing and tempering temperatures [22,34], regardless of whether the CT is carried out after quenching of after tempering.

The aim of the present research is to evaluate the effect of a tailored heat treatment on the microstructure and mechanical behaviour of the Böhler K890 Microclean PM tool steel [37]. This heat treatment includes a cryogenic step before the last tempering. The study compares the microstructure and final performance induced by this new heat treatment with those produced by a conventional heat treatment, and it focuses on its influence on the fatigue strength of unnotched and notched steel. Moreover, the experimental fatigue notch factor (Kf) of this tool steel has been compared to the data obtained by several empirical relationships, widely used in machine design, which assess the Kf on the basis of notch geometry and material strength. The knowledge of reliable fatigue and Kf data, indeed, is

undoubtedly fundamental when designing complex multi-shaped mechanical components with the new generation of ultra-clean PM tool steels.

2. Material and Methods

2.1. Material

In this work, the Böhler K890 Microclean (Voestalpine Böhler Edelstahl GmbH & Co KG, Linz, Austria) [37] cold work tool steel was investigated under two different heat treatment conditions. The steel, produced via PM, was acquired as annealed bars (diameter 40 mm) obtained by hot working after the HIP phase.

The chemical composition, evaluated by a glow discharge optical emission spectroscope (GD-OES) Spectrum GDA 650 HR Analyser (Spectruma Analytik GmbH, Hof, Germany) according to ISO 14707 [38] standard, is reported in Table 1.

Table 1. Chemical composition (wt%) of the studied Böhler K890 Microclean steel.

C	Mn	Si	Ni	Co	Mo	V	W	Fe
0.80 ± 0.02	0.35 ± 0.01	0.59 ± 0.01	4.14 ± 0.04	3.90 ± 0.02	2.99 ± 0.01	2.30 ± 0.03	2.43 ± 0.01	Bal.

The steel underwent two different heat treatments, schematically shown in Figure 1. The first (hereafter referred to as "K890-I") consists of: i. austenitizing (after two preheating stages at 650 and 850 °C for 2 h) at 1070–1100 °C for 30 min; ii. gas quenching by nitrogen at 5 bar; iii. triple tempering at 540–560 °C for 2 h. The second heat treatment (hereafter referred to as "K890-II") consists of: i. austenitizing (after two preheating stages at 650 and 850 °C for 2 h) at 1150–1180 °C for 30 min; ii. gas quenching by nitrogen at 5 bar; iii. double tempering at 510–520 °C for 2 h; iv. cryogenic treatment in nitrogen at −80 °C for 2 h; iv. final tempering at 520–530 °C for 2 h. While K890-I is the conventional heat treatment for this tool steel, K890-II is a new solution.

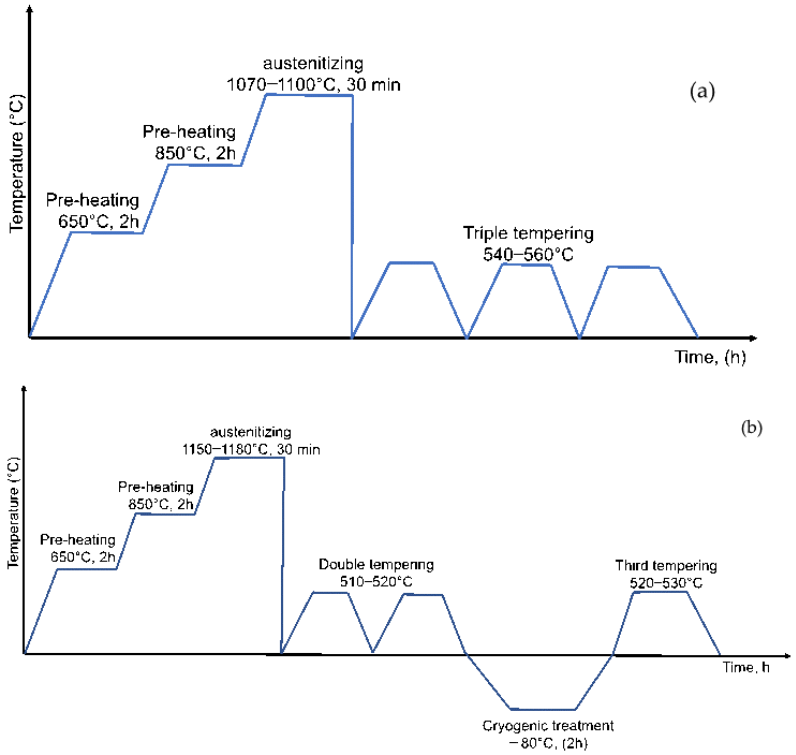

Figure 1. Schematization of K890-I (**a**) and K890-II (**b**) heat treatments.

In the K890-II, the austenitization temperature was raised compared to the K890-I and the cryogenic step was carried out after the second tempering with the aim at improving the steel toughness by reducing the amount of primary carbides and increasing the amount of secondary carbides. The tempering temperatures of K890-II, in contrast, were reduced with the purpose of increasing steel hardness and strength. However, both K890-I and K890-II include multiple tempering in order to reduce the amount of retained austenite.

2.2. Microstructural Characterization

Microstructural characterization of the heat-treated steel was carried out on metallographic samples cut from tensile and fatigue specimens. At least 10 metallographic samples were analyzed for K890-I and K890-II. Analyses were carried out by means of a Zeiss Axios optical microscope (OM), a Zeiss EVO50 scanning electron microscope (SEM) (Carl Zeiss Microscopy GmbH, Oberkochen, Germany) equipped with an Oxford Instrument INCA X-Act PentaFet Precision energy dispersive spectroscope (EDS) (Oxford Instruments Industrial Products Limited, Oxon, England), and a FEG SEM TESCAN MIRA (Tescan Orsay Holding a.s., Brno-Kohoutovice, Czech Republic) equipped with a Bruker Q200 EDS (Bruker Corporation, Billerica MA, USA). The metallographic samples were prepared according to the ASTM E3 standard [39] and chemically etched with Nital 2% solution (100 mL ethanol and 2 mL nitric acid) for a few seconds, according to the ASTM E407 standard [40].

The average size of the carbides and the austenitic grains was estimated by image processing, at the same magnification, of ten representative SEM images of metallographic samples.

The volume fraction of retained austenite was evaluated according to the ASTM E-975-13 standard [41], using a Philips PW1710 X-ray diffractometer (Koninklijke Philips N.V, Eindhoven, the Netherlands), radiation Co Kα1 = 1.78901 Å with 35 kV and 30 mA; Fe filter for Kβ suppression. The data were processed with e X'Pert HighS-core Plus, software (v. 2.2.0, Malvern Panalytical Ltd, Malvern, UK)

2.3. Mechanical Tests

The mechanical behaviour of the steel was studied by means of nanoindentation, hardness, tensile and fatigue tests on notched and unnotched specimens.

Nanoindentation tests were carried out according to ISO 14577 [42] in load control mode using a calibrated Ultra Nanoindenter (UNHT) (CSM Instrument, Neuchatel, Switzerland) equipped with a Berkovich diamond tip, at a constant loading rate of 200 $\mu N \cdot s^{-1}$, up to a maximum load of 30,000 mN. The 50 s total indentation time was divided into three segments, consisting of 20 s loading and unloading, and 10 s holding time. The tests were performed by creating two 10 $\times$ 10 grids of indents, 100 μm spaced, for a total of 200 indents for each sample. During the test, the nanoindenter continuously recorded the penetration depth and the load. More details on the nanoindentation test are discussed in [43,44] where it is explained how it is possible to calculate Indentation Hardness HI (GPa) plastic deformation work Wp (pJ) and total deformation work Wt (pJ). High Wt values mean high energy dissipated by the material during loading which is related to high toughness.

Hardness measurements (HV30) were carried out according to the Vickers test method described in ISO 6507-1 standard [45], using a 30 kg load and 10 s duration time.

The tensile properties (yield strength (YS), ultimate tensile strength (UTS) and elongation to failure (E%)) were evaluated on proportional round specimens (5 mm diameter and 25 mm gauge length), using a servo-hydraulic testing machine according to EN ISO 6892 standard [46]. Three specimens for each of the two investigated heat treatment conditions were tested.

Fatigue tests were carried out according to ISO 1143 [47] on unnotched and notched specimens (Figure 2), using a four-point rotating bending testing machine at a frequency of 50 Hz. The stress concentration factor induced by the notch was evaluated as equal to K_t = 3 and K_t = 3.1 on the basis of the findings of Noda [48] and Young [49], respectively.

The fatigue strength was evaluated at 10^7 cycles, in accordance with the staircase method reported in the ISO 12107 [50] standard, using 15 specimens and a 50 MPa stress step.

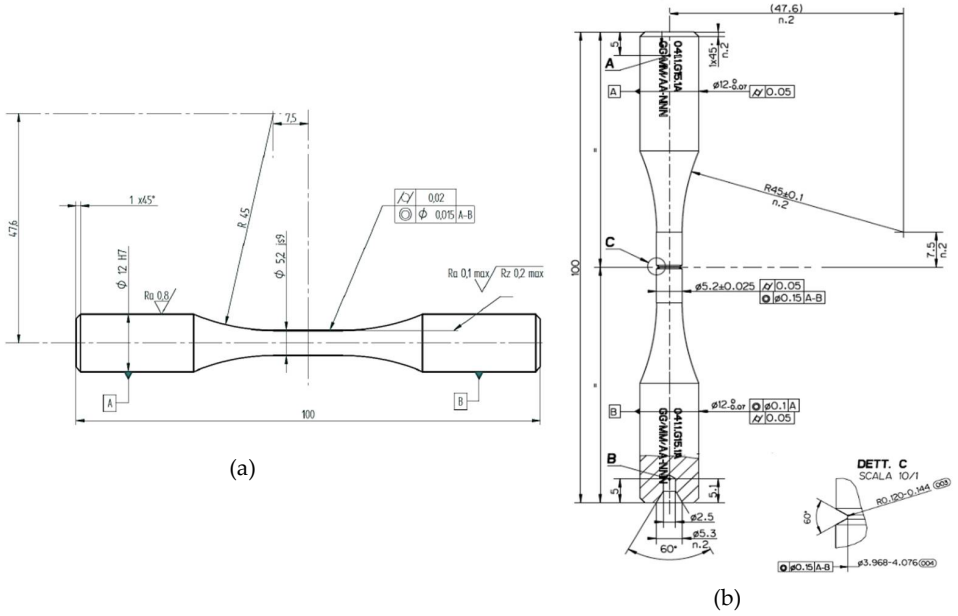

(a) (b)

Figure 2. Shape and dimensions (mm) of the rotating bending fatigue test specimens: (**a**) unnotched and (**b**) notched (in this figure the commas has been used as decimal sign).

The unnotched specimens were machined before the heat treatment and subsequently were surface finished to obtain an average roughness of Ra = 0.1 μm in the gauge length. The notches were completely machined after the heat treatment, and finished to a surface roughness Ra in the range of 0.2–0.4 μm. Roughness measurements were carried out with a stylus profilometer (tip radius of 5 μm), according to DIN-4768 [51].

Notch and fracture surface analyses were carried out by means of a Hirox KH 7700 3D-digital microscope (Hirox Co. Ltd., Tokyo, Japan) and SEM equipped with Zeiss EVO50 (Carl Zeiss Microscopy GmbH, Oberkochen, Germany), respectively.

3. Results

3.1. Microstructure

Representative optical and scanning electron micrographs of the investigated PM tool steel, after K890-I and K890-II heat treatments, are presented in Figures 3–5. Microstructures consist of homogeneous fine tempered martensite with dispersed MC (dark grey in Figures 4 and 5) and M_6C (white in Figures 4 and 5) carbides [21,22,24,25]. The prior austenite grain size in the K890-I and K890-II is comparable and it ranges between (4 and 9 μm), regardless of the different austenitization temperature. Moreover no retained austenite (RA), segregations, inclusions, porosity, carbides larger than 2 μm or carbides clusters were detected by metallographic analyses (Figures 3 and 4).

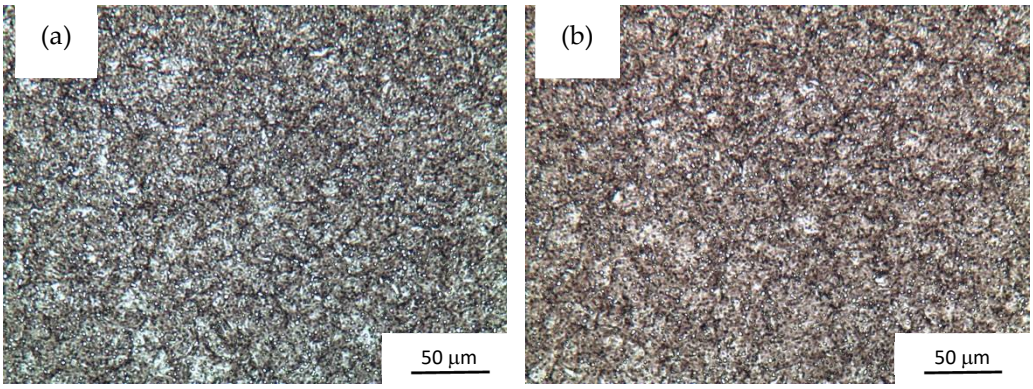

Figure 3. Optical micrographs of K890 Microclean steel after: (**a**) conventional K890-I and (**b**) K890-II heat treatment.

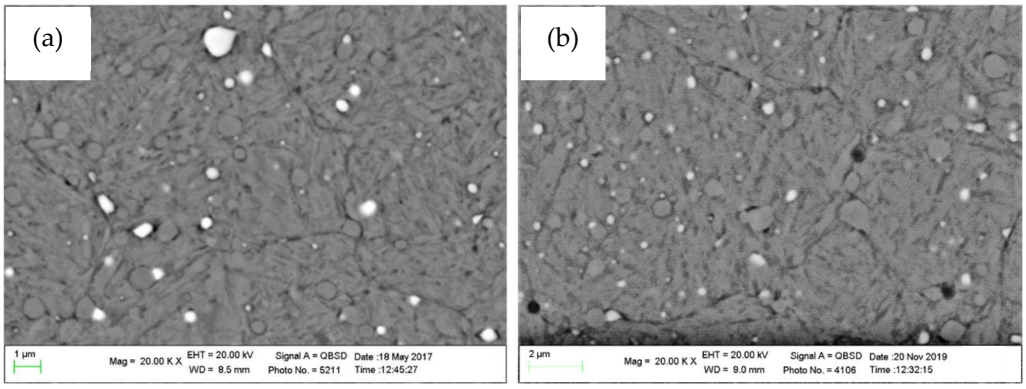

Figure 4. SEM-BSE representative micrographs of sample treated according to K890-I (**a**) and K890-II (**b**).

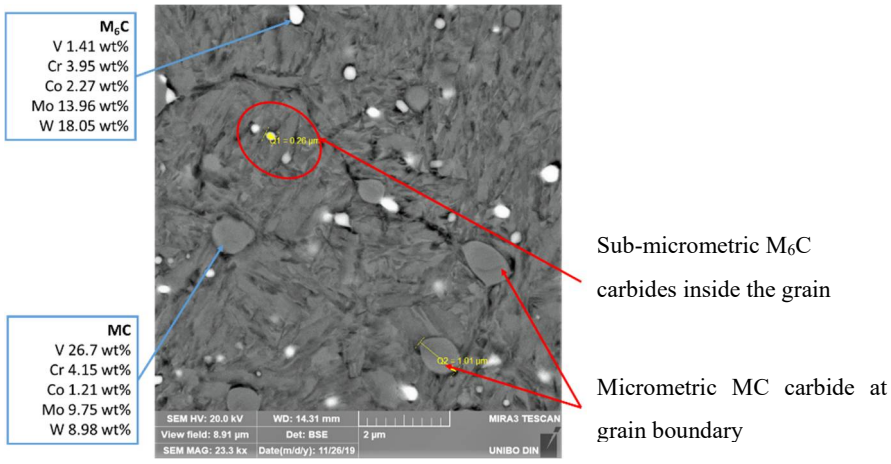

Figure 5. Representative SEM-BSE micrograph of the K890-II treated steel with MC carbides along grain boundaries and M6C carbides inside grains. The light grey carbides, M6C type, are Mo and W rich, while the dark grey carbides MC type are V rich.

MC carbides (Figures 4 and 5) are mainly micron-sized, distributed along the primary austenite grain boundaries and with high V content, while M6C carbides, with sub-micrometric size, also develop inside the grains and are Mo and W rich [23,25].

Despite the different austenitizing temperatures, the differences between the average size of the carbides in the K890-I and K890-II treated sample is negligible, as observable in

Figure 5 and supported by the distribution of carbide size reported in Figure 6. According to the carbides' distribution curves, the mean value of carbide size is about 0.40 µm with a standard deviation of about 0.10 µm for both K890-I and K890-II treated samples. The only remarkable differences concern the area fraction and the maximum size of the carbides equal, respectively, to 5.20 ± 0.50 and 1.38 µm for the K890-I and 4.40 ± 0.70 and 1.11 µm for and K890-II treated samples. OM and SEM analyses, instead, were not able to show the presence of secondary carbides developed during tempering and/or CT soaking.

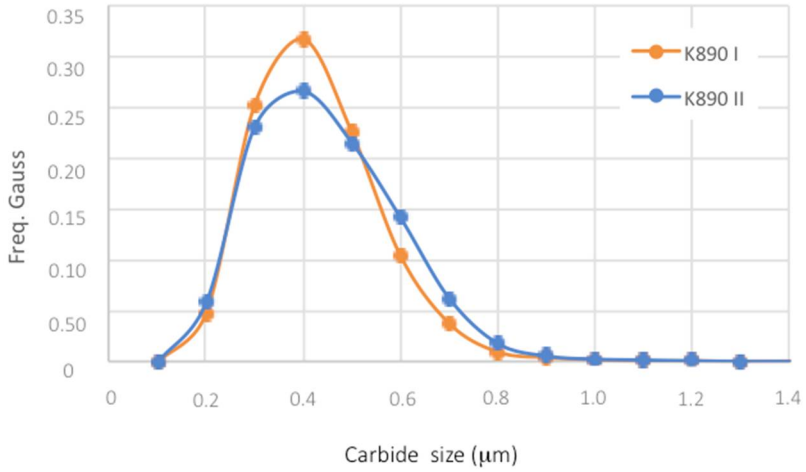

Figure 6. Gaussian distribution of carbides size in K890-I and K890-II specimens. K890-II presents smaller carbides size (peak value) and a more homogeneous (amplitude) carbide distribution.

Finally, XRD patterns (Figure 7) confirm that the amount of retained austenite is negligible and is lower than the detection threshold of the equipment (about 1.5%) in both K890-I and K890-II investigated specimens.

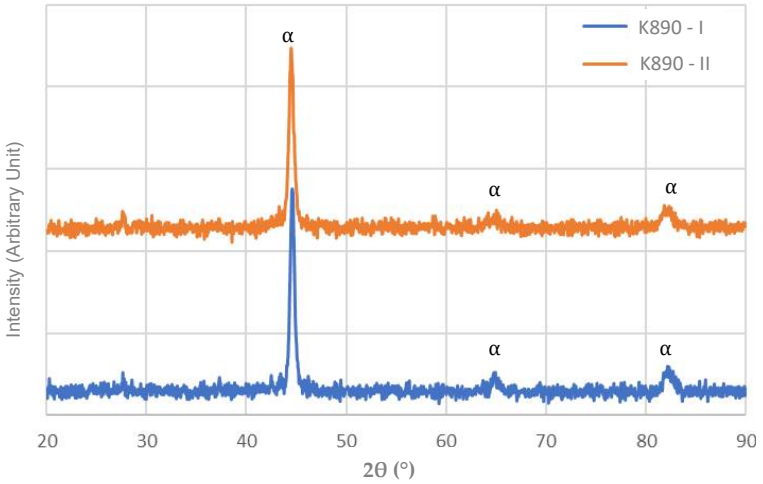

Figure 7. XRD patterns of samples subjected to K890-I and K890-II treatments. The amount of retained austenite is lower than the detection threshold of the equipment for both heat treatments; therefore, no peaks related to the γ phase can be observed.

3.2. Hardness and Tensile Properties

The effects of the two heat treatments on hardness and tensile behaviour are summarized in Table 2, while an example of tensile curves is reported in Figure 8.

Table 2. Hardness and tensile properties (mean values and standard deviations) of the K890 steel subjected to K890-I and K890-II heat treatments.

	HV30	YS (MPa)	UTS (MPa)	A% (%)
K890-I	741 ± 3	2153 ± 20	2513 ± 10	2.1 ± 0.1
K890-II	817 ± 17	2381 ± 15	2848 ± 22	2.3 ± 0.1

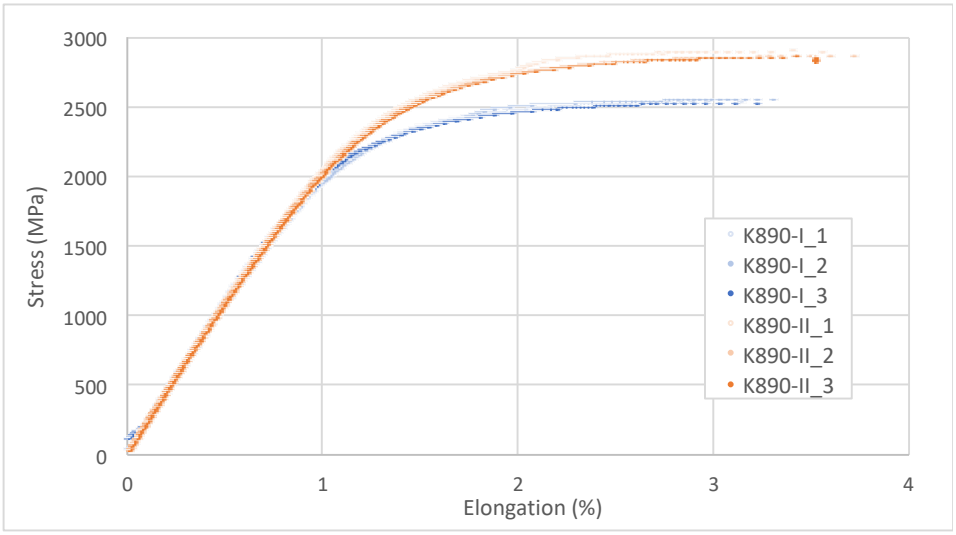

Figure 8. Comparison of stress-elongation curves of the K890 steel subjected to K890-I and K890-II heat treatments.

The data point out that K890-II leads to increased hardness (about 10% more), greater strength (about 11% and 13% more for YS and UTS, respectively) and a slightly superior elongation to failure (about 7% more) compared to K890-I.

The higher hardness and strength of the K890-II compared to the K890-I steel can be explained by taking into account both the different austenitization and tempering temperatures as reported by [19–22]. The increase in austenitization temperature, indeed, leads to the solutioning of a higher amount of primary carbides, resulting in a higher carbon concentration in the martensite after quenching, and consequently its superior final hardness. Furthermore, the higher C supersaturation may have also promoted the precipitation of secondary carbides during the tempering and/or CT, which can induce a slight increase in hardness, since they are not affected by the subsequent tempering. In particular, as stated by [23,27], according to the nucleation and growth theory, precipitation of secondary carbides can take place during heating from cryogenic temperature to room temperature and the subsequent tempering.

In addition, as is well known, the lower tempering temperature of K890-II compared to K890-I (520–530 °C and 540–560 °C respectively), contributes to increases in the degree of its hardness [52,53].

It is worth noting that, despite its higher degree of hardness, K890-II also exhibits a slightly higher elongation to failure. This result is in agreement with the findings reported in [26–28,34,35], in which the authors state that the precipitation of secondary carbides during the CT can reduce the carbon supersaturation in the martensite, decreasing residual stresses and improving ductility and toughness, resulting also in a general decrease of microcracking tendency.

In addition, the homogenous microstructure observed in both K890-I and K890-II leads to a negligible scatter of the results with a standard deviation lower than 1% for hardness, UTS and YS.

3.3. Nanoindentation

The nanoindentation technique is widely used because of its ability to measure the mechanical properties of a small volume of material. It allows the Indentation Hardness (HI), Total hardening Work (Wt) and plastic Work (Wp) to be evaluated by analysing the load—penetration depth curve. HI—similar to the other micro or macro hardnesses—provides information on the material strength; Wt expresses the ability of materials to dissipate deformation energy during loading and, for this reason, is a useful tool to evaluate ductility and toughness, as reported in [43,54–56].

An example of load—penetration depth curves by nanoindentation tests for the investigated steels is reported in Figure 9. The results were statistically analysed and their gaussian distributions are shown in Figure 10, while the mean values and standard deviations are summarized in Table 3. It can be clearly seen that K890-II increases Indentation Hardness (HI), total hardening work (Wt) and plastic work (Wp), in comparison to K890-I (by about 15%, 4% and 10% respectively). As reported in [43,54], the higher the Wt and Wp values, the greater the ductility and toughness of the material. The results of nanoindentation confirm the increase of strength and ductility induced by the K890-II, already highlighted by the tensile tests.

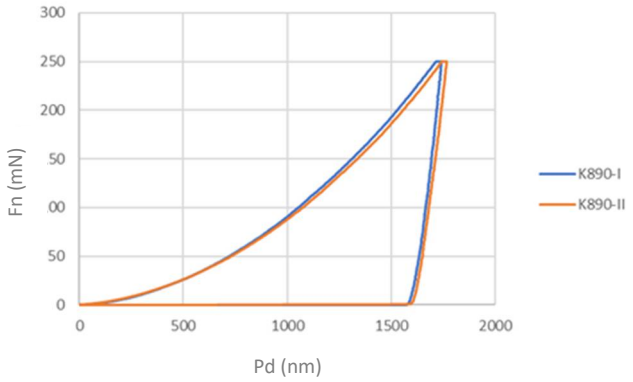

Figure 9. Nanoindentation load (Fn) vs. penetration (Pd) curves of K890-I and K890-II samples.

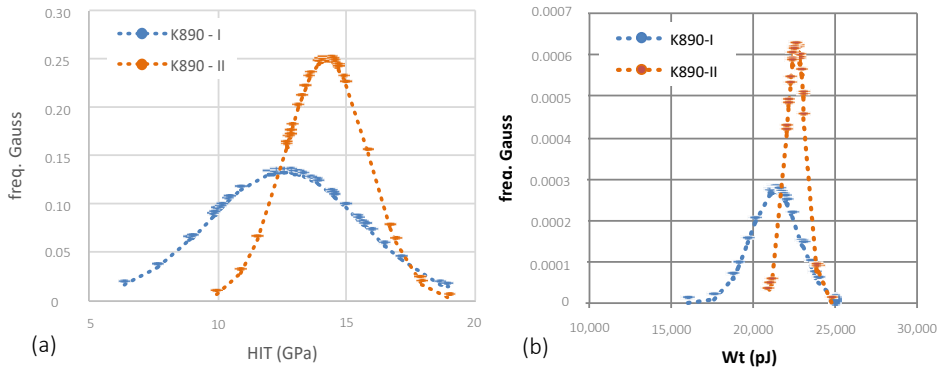

Figure 10. Gaussian distribution of HI (**a**) and Wt (**b**). In both graphs, the peak corresponds to the mean value and the curve amplitude to the standard deviation.

Table 3. Indentation Hardness (HI), Total hardening Work (Wt) and plastic Work (Wp) obtained by nanoindentation tests (mean values and standard deviations).

	HI (GPa)	Wt (pJ)	Wp (pJ)
K890-I	12.5 ± 1	21,400 ± 875	15,171 ± 135
K890-II	14.4 ± 2	22,268 ± 220	16,635 ± 160

It is worth noting that gaussian distributions of HI and Wt highlight the positive effect of a homogeneous microstructure in reducing the scatter in the mechanical properties of the investigated tool steel.

3.4. Fatigue Behaviour

The fatigue strength of notched and unnotched specimens was evaluated by rotating bending fatigue tests carried out following the staircase method, described in detail in ISO 12107 standard [50]. According to this method, the specimens are tested sequentially, starting from a defined stress for the number of cycles of interest or until failure, whichever comes first. In the present work, the stress has been chosen close to the expected steel fatigue strength, identified on the base of previous tensile tests and literature review. If the specimen fails the stress is decreased of a fixed step, if it survives the stress is increased of the same step. Commonly, this stress step is close to the expected standard deviation of the fatigue strength. According to this method at least 15 samples have to be tested to obtain accurate mean fatigue strength and standard deviation at the fixed number of cycle.

Images of the machined notches, obtained by 3D-digital microscope, are reported in Figure 11; the average surface roughness Ra of the notches ranges between 0.2 and 0.4 µm.

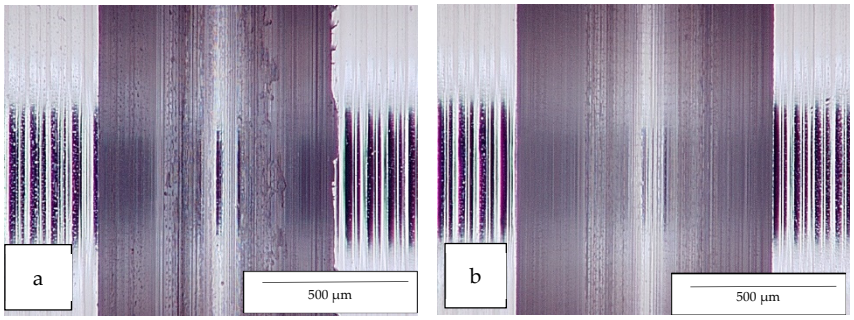

Figure 11. Representative images of the surface finishing of the notches for the (**a**) K890-I and (**b**) K890-II fatigue samples.

The results of the fatigue tests are summarized in Table 4, where the fatigue strength of notched S'ek and unnotched S'e specimens, the theoretical stress concentration factor for notched specimens K_t (estimated according to Noda [48] and Young [49]), and the fatigue notched factor K_f (ratio between S'e and S'ek [57]) are reported.

Table 4. Results of bending fatigue tests carried out on notched $S'e_k$ and unnotched specimens S'e; fatigue strength at 10^7 cycles for a failure probability of 50%. K_t is the theoretical stress concentration factor; K_f is the fatigue notch factor.

	$K_{t\ estimated}$	S'_e (MPa)	S'_{ek} (MPa)	$K_f = \frac{S'_e}{S'_{ek}}$	$\frac{S'e}{UTS}$
K890-I	3	1186 ± 29	525 ± 26	2.25	0.47
K890-II	3	1314 ± 39	692 ± 31	1.9	0.46

The experimental data point out the positive impact of the K890-II treatment on fatigue behaviour of the PM tool steel for both unnotched and notched specimens, as already observed for the static properties. Similar findings are also reported by [22,23,25] where the authors explain the effect of cryogenic treatment on the mechanical properties of tool steels. The K890-II unnotched samples have a fatigue strength 15% higher than the K890-I ones, while the K890-II notched samples have a fatigue strength approximately 25% higher than the K890-I ones.

Moreover, as also observed for static mechanical properties, the substantial absence of segregations, large carbides or carbides clusters and porosity, in both K890-I and K890-II, leads to a low scatter of the results of fatigue tests. As a matter of fact, the standard

deviation for the unnotched samples is lower than 3% while for the notched samples is lower than 5%.

3.5. Fracture Surface Analyses

Different fracture surface appearances were detected in unnotched and notched specimens, especially for the nucleation stage.

The fracture mechanisms of high strength tool steels are widely described in the literature [8,11,12,18,58]. According to the findings of the researchers, the main microstructural features that influence the fatigue behaviour of these steels are: large primary carbides, carbides clusters, inclusions (mainly aluminium-oxide or calcium-sulphides), segregations and voids [18]. All these features act as fatigue nucleation sites and reduce the cycles needed for initiating the crack in the material stage that requires the largest part of the total fatigue life [58]. For these steels, therefore, the improvement of fatigue behaviour is mainly achieved by promoting the development of a fine and homogeneous and microstructure.

Fracture surface analyses of the K890 I and K890 II confirmed these statements and, moreover, highlighted the different fracture nucleation mechanisms between unnotched and notched specimens.

Fracture surfaces of the unnotched samples are substantially flat and smooth, without evidence of plastic deformation even if the nucleation sites, the propagation and failure regions are clearly visible (Figures 12 and 13). In the samples in Figure 12 the absence of large microstructural defects and the small size of carbides leads to the development of crack initiation sites in the surface region (Figure 12) due to a flaw (Figure 12c–e) or to the accumulation of dislocation in slip bands (Figure 12a,b) [18]. However, the analyses highlighted that, in unnotched specimens, the cracks mainly originate from internal inclusions, showing a classical fish-eye morphology (Figure 13), despite no inclusions being observed by metallographic analyses because of their very low amount. Fish-eyes have been widely described and several studies have been carried out to investigate their formation and features [9,11,12,58]. All these studies agree with the fact that fish-eyes: (i) mainly occur under high number of loading cycles (above to 10^6) in high strength steels and, in particular, tool steels; (ii) develop in correspondence with carbides clusters, primary large carbides or non-metallic inclusions, due to both particle cracking and debonding; (iii) their typical features are the result of different crack growth mechanisms that take place during the early stages of crack propagation within the fish-eye.

According to [11,12], in presence of a fish-eye, the stage corresponding to the fish-eye growth takes up almost the total fatigue life of samples/components. Only when the fish-eye reaches a critical size (depending on loading and material properties) does the crack growth rate increase, until the moment final failure takes place (Figure 14). This final stage of the sample fatigue life happens remarkably fast while also taking up less than 1% of total fatigue life. In the presence of surface defects (or flaws), however, the higher stress-intensity factor induced by the defect (or flaw) allows the critical crack to grow faster than the fish-eye, reducing the cycles required for the crack initiation phase [12,58].

It should be noted that for both K890-I and K890-II samples, the fish-eye did not develop close to the surface, despite rotating bending fatigue tests inducing maximum stress on the surface of the specimen. This is probably due to the presence of surface compressive residual stresses, induced by the machining processes for sample production, which inhibit the crack of inclusions or carbides or their debonding from the matrix. Similar findings have also been reported in [7,9,18,59–61].

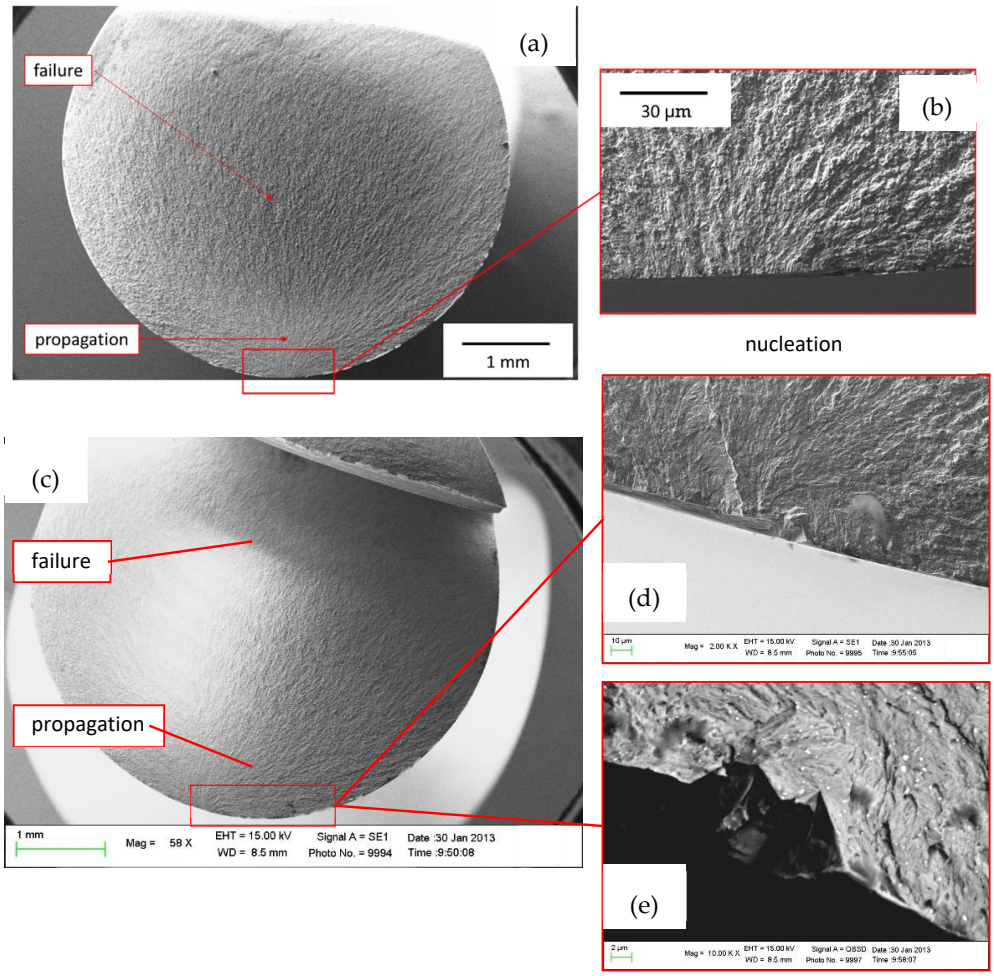

Figure 12. Fatigue fracture surface of unnotched samples. (**a**,**b**) crack initiation sites in the surface zone due to the accumulation of dislocation in slip bands (MPa 1150, cycles $7.5 \cdot 10^6$) and (**c**–**e**) presence of a flaw (MPa 1100, cycles $6.9 \cdot 10^6$).

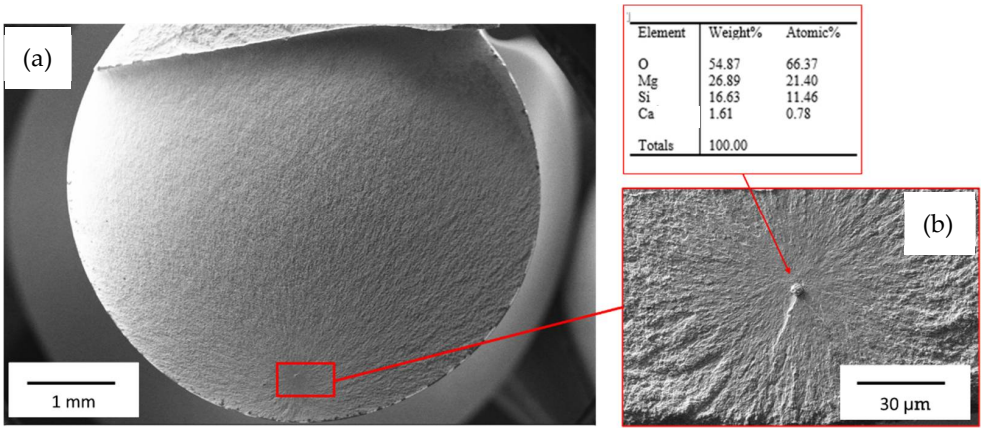

Figure 13. SEM-SE low magnification fatigue fracture surface of an unnotched sample (MPa 1100, cycles $5.4 \cdot 10^6$) with the crack initiation site in the sub-surface zone (**a**) and high magnification of the "fish-eye" with corresponding SEM-EDS analysis of non-metallic inclusion from which developed the "fish-eye" (**b**).

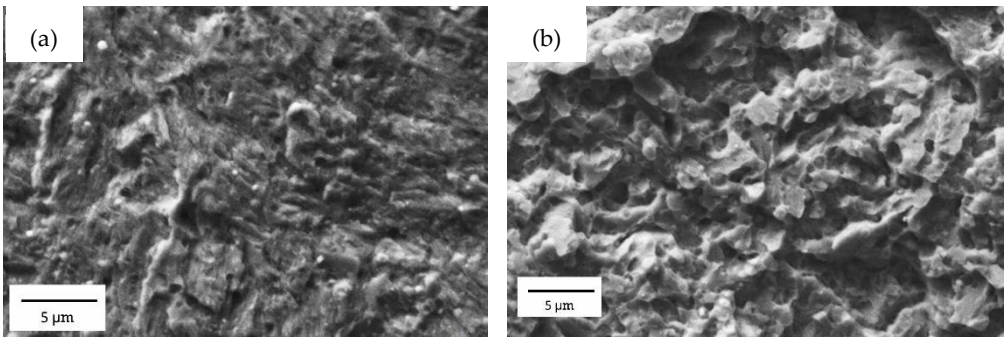

Figure 14. SEM-SE micrographs of smooth propagation zone (**a**) and rough final failure zone (**b**) of an unnotched sample.

Due to the high strength and low ductility of the tested steel and the high crack propagation rate, no clear fatigue striations are detected in the propagation region, even at high magnification, and no clear boundary between the crack propagation and final failure regions has been observed (Figure 14); the transition between the smooth surface present in the propagation region close to the fish-eye and the rough surface of the final failure is continuous. Moreover, no clear effects of the microstructure on the crack path were highlighted by the fractographic analyses, in agreement with the statements of Shiozawa et al. [10]. In particular, because of their small size, no fractured carbides were observed both in the propagation and in the final failure zone, in which the fine microstructure leads to the formation of micrometric and submicrometric dimples. On the contrary, in the notched specimens, the high surface stress concentration induced by the notch promotes the development of multiple initiation sites (even if no large carbides, inclusions, or voids have been detected) (Figure 15) [62] or single surface initiation sites close to the machining flaws of the notch root (Figure 16). In the first case, the cracks develop on different planes and connect during the final failure of the specimen.

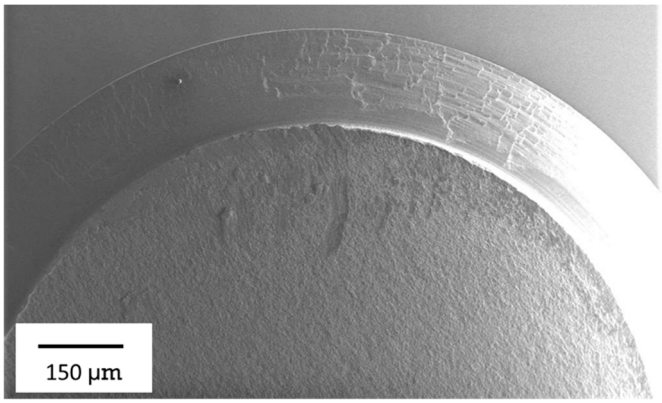

Figure 15. SEM-SE micrographs of multiple crack initiation sites in notched specimen. The outermost zone of the fracture surfaces of the specimen was partially damaged by the final stage of fracture.

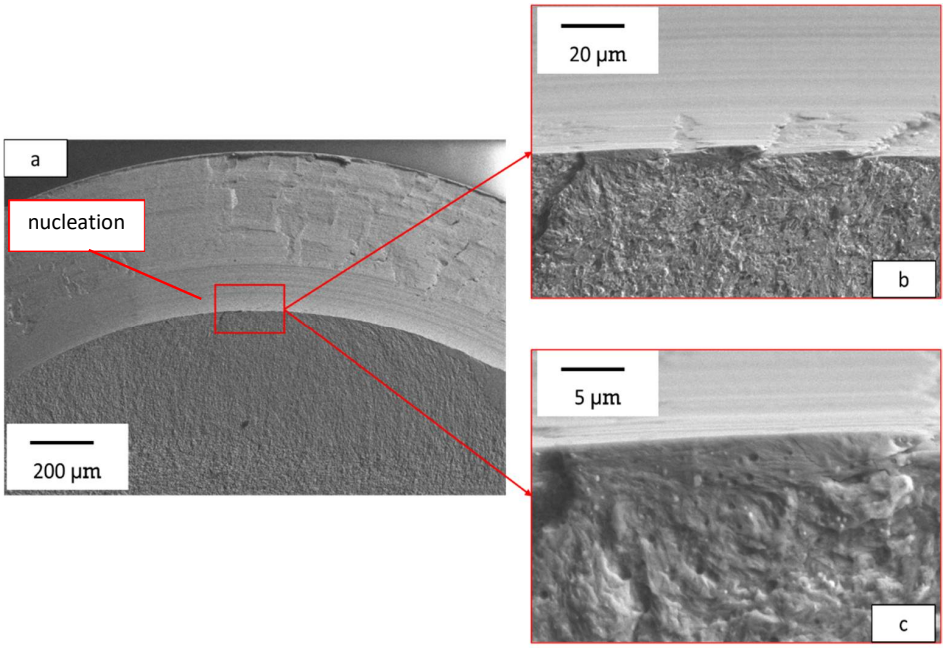

Figure 16. SEM-SE low magnification fractography of a notched sample (**a**) and high magnification of the crack nucleation site in correspondence of machining flaws of the notch root (**b**,**c**).

The morphologies of the fracture surfaces in the propagation and failure zones, however, are comparable to the corresponding areas of the unnotched specimens (Figure 17).

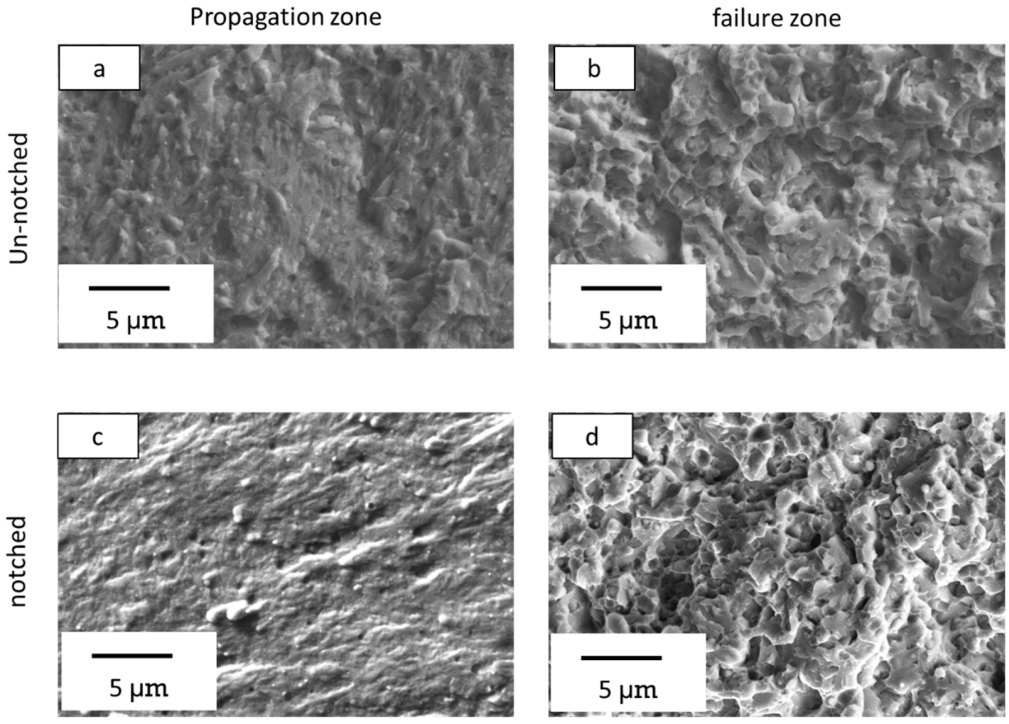

Figure 17. SEM-SE micrographs of propagation and failure zone of unnotched (**a**,**b**) and notched samples (**c**,**d**).

4. Discussion

Although the authors are fully aware that a thorough understanding of the effect of the two heat treatments on the microstructure, in particular on the formation of secondary

carbides, can only be provided by TEM analyses, a possible explanation of the positive effect of K890-II heat treatment on the microstructure and mechanical behaviour of PM K890 tool steel is proposed, based on a bibliographic survey.

It is widely recognized [24,26–32] that heat treatment optimization of tool steels is often aimed at reaching a compromise between the need to: (i) increase hardness and strength; (ii) ensure adequate toughness; (iii) reduce the amount of retained austenite.

Therefore, in conventional quenching and tempering heat treatment, the austenitization temperature is defined in order to avoid an excessive dissolution of primary carbides, and the consequent carbon enrichment of the austenite. As a matter of fact, high C content leads to the formation of harder and thus more brittle martensite and increases the amount of retained austenite (RA) after quenching. In order to enhance toughness and to reduce the amount of retained austenite, high strength steel generally undergoes multiple tempering cycles, at a relatively high temperature, in order to transform RA and to obtain a tougher tempered martensite. In fact, the presence of the metastable retained austenite reduces steel hardness, toughness and fatigue strength [24,26,28,31], since it may transform into brittle martensite in working conditions [27,29,34,35,63–65].

The cryogenic heat treatment, carried out after quenching or after tempering, allows these limits to be exceeded. In point of fact, during the cryogenic phase of the heat treatment, the transformation of RA into martensite takes place and secondary fine carbides are formed. These are in addition to the secondary carbides that develop during tempering, and increase mechanical properties, toughness, and wear resistance [22,63,64]. The microstructural evolution and the carbides precipitation induced by cryogenic treatment in tool and high carbon steels in particular, is discussed by several authors, such as Gavriliuk et al. [66], Patil [22] and Das [63,64]. These authors demonstrate that carbon atoms are immobile at temperatures below −100 °C. However, during the heating up to room temperature from cryogenic and during subsequent tempering, ageing of the carbon-supersaturated martensite (starting from −50 °C) leads to martensite decomposition. This induces precipitation of submicrometric carbides with a reduction of the compressive residual stresses according to [65,67].

However, the formation of these fine and homogeneously dispersed carbides has a positive effect on the ductility and toughness of the steel that compensates the effect of the reduction of compressive residual stresses on the fatigue behavior [9,65,67]. In the light of the above, the austenitization temperature can be increased and the tempering temperature reduced when a cryogenic treatment is applied, since a higher amount of C in solid solution in the austenite before quenching and a lower tempering temperature are no longer critical for the final toughness of the steel.

As a result, the new K890-II treatment that is proposed can lead both to an increase in the hardness and strength of steel and a slight increase in its ductility, toughness and fatigue strength.

The synergic positive effect of increasing the austenitizing temperature, reducing the tempering temperature and cryogenic treatment on the mechanical performance of the investigated tool steel is confirmed by the results of hardness and tensile tests. As a matter of fact, K890-II treated steel, has a higher degree of hardness, YS and UTS (10, 11 and 13% respectively) and even a slightly superior elongation to failure (2.3 vs. 2.1%) compared to K890-I treated steel.

These results are corroborated by the indentation tests data, which highlight that the combination of a higher austenitizing temperature, cryogenic treatment and a lower tempering temperature increases the Indentation Hardness of the K890 steel without decreasing its toughness, in terms of energy absorbed by the material during the deformation. Indeed, K890-II has higher total hardening work (Wt) compared to K890-I steel, and this is probably due to the reduction of its tendency to microcrack, induced by the lower residual stress resulting from the lower supersaturation of martensite due to the precipitation of fine carbides during cryogenic treatment [33,35]. Moreover, it is well known [67] that a re-

duction in the maximum carbide size reduces the probability of fracture and/or debonding from the matrix, and can therefore further increase steel toughness.

As for fatigue behaviour, the increase in the static strength of the K890-II treated steel leads to a proportional increase in the unnotched fatigue strength (S'e) equal to 1314 MPa for K890-II and 1186 MPa for K890-I, with a S'e/UTS ratio of about 0.47 for both K890-II and K890-I steels. As reported in [68–71], a similar S'e/UTS ratio suggests that similar fatigue failure mechanisms take place. This statement is in agreement with the fracture surface analyses already described in Section 3.5. In fact, according to these, the crack nucleation sites in both K890-I and K890-II unnotched samples were primarily characterized by the presence of fish-eyes, mainly developed in correspondence with small inclusions, while the propagation stage of the fracture took place with a high propagation rate, so that even at high magnification no fatigue striations were detected.

It can seem, therefore, that the increase in the S'e value of the K890 unnotched samples is largely due to the increase in its hardness and strength, which mainly influences the initiation phase of the cracks, while no effect can be attributed to the toughness.

The importance of steel toughness on the fatigue strength of K890 steel becomes instead clear by comparing the fatigue notch factor K_f, for both the K890-I and K-890-II notched samples.

The fatigue notch factor K_f for metallic materials measures the reduction in the fatigue strength of a sample due to the presence of a notch, and is defined as the ratio of the fatigue strength of the unnotched specimen (S'e) to the fatigue strength of the notched specimen (S'ek) [57]:

$$K_f = \frac{\mathrm{S'e}}{\mathrm{S'ek}} \tag{1}$$

The K_f coefficient is obtained experimentally and depends on steel chemical composition, heat treatment, type of notch and geometry of the specimen. Its value ranges between 1 (material notch- insensitive) and the theoretical stress concentration factor K_t (material fully notch-sensitive).

K_t is the ratio between the greatest elastically calculated stress in the region of the notch (or other stress concentrators) to the corresponding nominal stress. K_t is a theoretical factor that depends only on the geometry of the notch and the type of stress (normal stress, bending or torsion) [57].

Experimental tests show that in most cases K_f is less than K_t because metals locally undergo stress values higher than their yield strength, and therefore a local plasticization of the material and a redistribution of the stresses occurs at the notch root. The fatigue limit of the notched components cannot therefore be evaluated solely by considering the maximum theoretical value of the tension σ_{max} at the notch [60] but the stress gradient, the ductility and the toughness of the material also have to be considered because of their influence on both crack initiation, from defects or surface discontinuities, and their subsequent growth [68–70].

In order to consider these aspects Khun [69] developed the following relationship:

$$K_f = 1 + q(K_t - 1) \tag{2}$$

where the notch sensitivity parameter q ranges between 0 and 1 and takes into account both the notch geometry and the mechanical performances of the material. This parameter is assumed to increase with increasing UTS because, according to Khun [69], an increase of UTS corresponds to a decrease of ductility and toughness.

Based on similar considerations, several empirical relationships were developed between the 1930s and 1970s to evaluate q on the basis of notch geometry and UTS.

According to Neuber [71]:

$$q = \frac{1}{1 + \frac{\pi}{\pi - \omega}\sqrt{\frac{A}{r}}} \tag{3}$$

And therefore:

$$K_f = 1 + \frac{K_t - 1}{1 + \frac{\pi}{\pi - \omega}\sqrt{\frac{A}{r}}} \tag{4}$$

where ω is the notch flank angle, r is the notch root radius, and A is the Neuber constant, which is related to the tensile strength of the material. The $A^{1/2}$, in fact, can be approximated by a third-order polynomial fit of *UTS*.

According to Peterson [72]:

$$q = \frac{1}{1 + \frac{a}{r}} \tag{5}$$

And therefore:

$$K_f = 1 + \frac{K_t - 1}{1 + \frac{a}{r}} \tag{6}$$

where a is a material constant (in mm) and for the steels is defined as:

$$\mathrm{a} = 0.025\left(\frac{2070}{UTS}\right)^{1.8} \tag{7}$$

According to Heywood [73]:

$$K_f = \frac{K_t}{1 + \frac{2(K_t - 1)}{K_t}\frac{\sqrt{b}}{\sqrt{r}}} \tag{8}$$

where b (in mm) is a constant that takes into account both the material strength of *UTS* and the notch geometry. For the geometry of the notched fatigue specimens, b is given by:

$$b = \frac{104}{UTS} \tag{9}$$

A comparison of the experimental K_f coefficients (reported in Table 5) highlights that the increase of ductility and toughness induced by the K890-II compared to K890-I treatments leads to lower K_f values. Furthermore, the comparison of the experimental K_f coefficients with those calculated according to previous relationships, emphasises again the importance of considering not only *UTS* for new PM tool steels, as in the past, but also ductility and toughness, in order to correctly assess their fatigue behaviour in the presence of notches. It is worth noting that the Neuber relationship (4) cannot be applied to the K890 steel since for high *UTS* it yields $K_f > K_t$, while Peterson and Heywood relationships overestimate the fatigue notch sensitivity of the K890 by about 30%. As shown in Table 5, K_f values for K890 can be, alternatively, more accurately predicted by the relationship (10) developed by Hu and Cao [70] for low notch sensitivity materials, which considers the deformation and strain hardening behaviour of the material rather than the *UTS*.

$$K_f = K_t^{2/(3+n)} \tag{10}$$

where n is the strain hardening coefficient and can be evaluated by means of the following relationship [74]:

$$n = 1 - \left(\frac{YS}{UTS}\right)^2 \tag{11}$$

Table 5. Notch factor K_f values for the K890-I e K890-II treated steel evaluated by means of empirical (Peterson [72], Heywood [73], Hu and Cao [70]) and experimental relationships.

	Peterson (Empirical)	Heywood (Empirical)	Hu and Cao (Empirical for Low Notch Sensitivity Materials)	Experimental
K890-I	K_f=2.8	K_f=2.6	K_f=2.0	K_f = 2.2
K890-II				K_f = 1.9

As reported by Hu and Cao [70], because n represents the homogeneous deformation due to strain hardening, the greater the n, the greater the possibility of homogeneous deformation, and the greater the decrease in stress concentration at the notch root.

Despite its high strength, K890 steel exhibits lower fatigue notch sensitivity compared to traditional tool steels, thanks to its increased ductility and toughness, resulting from the steel production process, as well as from a proper optimization of the heat treatment parameters [9,18,22].

In fact, this positive combination of high strength, ductility and toughness, and the presence of fine carbides induced by the K890-II treatment actually prevents or slows down the nucleation of the cracks and their growth.

In the light of the above, and considering that K890 steel, in particular after K890-II treatment, has K_f values comparable with steels for structural applications [68,70], it is possible to infer that it could provide a viable option for the production of high performance components, even those with complex geometries, such as camshafts or crankshafts.

5. Conclusions

The aim of this present study is to evaluate the effect of an optimized heat treatment, including a cryogenic treatment before the last tempering, on microstructure and mechanical behaviour of the powder metallurgy K890 tool steel. Conventionally heat-treated steel (austenitizing at 1070–1100 °C for 30 min, gas quenching, triple tempering at 540–560 °C for 2 h, referred to as "K890-I") was compared with the same steel which underwent the new heat treatment (austenitizing at 1150–1180 °C for 30 min, gas quenching, double tempering at 510–520 °C for 2 h, cryogenic treatment in nitrogen at −80 °C for 2 h and final tempering at 520–530 °C for 2 h, referred to as "K890-II"). The following main conclusions can be drawn:

- The K890-II treatment improved tensile strength without decreasing elongation to failure, probably thanks to both a finer and more homogeneous carbide distribution into the martensite matrix and a decrease in martensite carbon supersaturation.
- Nanoindentation tests confirmed the tensile test data. The K890-II increased Indentation Hardness and indentation work compared to K890-I, which resulted in a reduction in microcracking tendency.
- Compared to the K-890-I treatment, the simultaneous higher strength, ductility and toughness induced by the K890-II treatment led to an increased fatigue strength for both the unnotched and notched specimens. Fatigue strength of the K890-II samples was about 15% and 25% higher for unnotched and notched samples, respectively, in comparison with the K890-I treatment.
- Fracture surface analyses showed that in unnotched specimens the cracks mainly originate from internal inclusions, showing a classical fish-eye morphology, while in the notched ones the cracks mainly develop from the surface.
- This present work demonstrates that the fatigue notch factor K_f of the K890 tool steel, after optimized heat treatment, is comparable with that of high strength steels. This makes K890 steel an highly attractive material for the production of high performance mechanical components, such as crankshafts.

Author Contributions: Conceptualization, A.M. and L.C.; methodology, A.M., L.C., S.M.; investigation, A.M., S.M.; data curation, A.M.; writing—original draft preparation, A.M.; writing—review and editing, A.M., L.C., S.M.; supervision, L.C. All authors have read and agreed to the published version of the manuscript.

Funding: This research received no external funding.

Institutional Review Board Statement: Not applicable.

Informed Consent Statement: Not applicable.

Data Availability Statement: Not applicable.

Acknowledgments: The authors would like to thank the following for their support of the experimental work: Andrea Morri and Ramona Sola at the Industrial Research Centre for Advanced Mechanics and Materials (CIRI-MAM); Giulia Baglieri and Giacomo Mazzola at the Department of Industrial Engineering (DIN) of the University of Bologna.

Conflicts of Interest: The authors declare no conflict of interest.

References

1. Available online: https://www.bohler-edelstahl.com/en/ (accessed on 7 July 2021).
2. Available online: https://www.erasteel.com/ (accessed on 7 July 2021).
3. Ceschini, L.; Morri, A.; Morri, A.; Messieri, S. Replacement of Nitrided 33CrMoV Steel with ESR Hot Work Tool Steels for Motorsport Applications: Microstructural and Fatigue Characterization. *J. Mater. Eng. Perform.* **2018**, *27*, 3920–3931. [CrossRef]
4. Beiss, P. Chemical Composition of Powder Metallurgy High-Alloy Tool Steels. In *ASM Handbook*; Samal, P., Newkirk, J., Eds.; ASM International: Materials Park, OH, USA, 2015; pp. 530–532. [CrossRef]
5. Schade, C. Introduction to Metal Powder Production and Characterization. In *ASM Handbook*; ASM International: Materials Park, OH, USA, 2015; pp. 55–57. [CrossRef]
6. Mashl, S.J. Powder Metallurgy Processing by Hot Isostatic Pressing. In *ASM Handbook*; ASM International: Materials Park, OH, USA, 2015; pp. 260–270. [CrossRef]
7. Garrison, W.M., Jr. Ultrahigh-strength steels for aerospace applications. *JOM* **1990**, *42*, 20–24. [CrossRef]
8. Meurling, F.; Melander, A.; Tidesten, M.; Westin, L. Influence of carbide and inclusion contents on the fatigue properties of high speed steels and tool steels. *Int. J. Fatigue* **2001**, *23*, 215–224. [CrossRef]
9. Melander, A.; Rolfsson, M.; Nordgren, A.; Jansson, B.; Hedberg, H.; Lund, T. Influence of inclusion contents on fatigue proper-ties of SAE 52100 bearing steels. *Scand. J. Metall.* **1991**, *20*, 229–244.
10. Shiozawa, K.; Morii, Y.; Nishino, S.; Lu, L. Subsurface crack initiation and propagation mechanism in high-strength steel in a very high cycle fatigue regime. *Int. J. Fatigue* **2006**, *28*, 1521–1532. [CrossRef]
11. Sohar, C.; Betzwar-Kotas, A.; Gierl, C.; Weiss, B.; Danninger, H. Gigacycle fatigue behavior of a high chromium alloyed cold work tool steel. *Int. J. Fatigue* **2008**, *30*, 1137–1149. [CrossRef]
12. Sohar, C.R.; Betzwar-Kotas, A.; Gierl, C.; Weiss, B.; Danninger, H. Fractographic evaluation of gigacycle fatigue crack nucleation and propagation of a high Cr alloyed cold work tool steel. *Int. J. Fatigue* **2008**, *30*, 2191–2199. [CrossRef]
13. Chapetti, M.D.; Tagawa, T.; Miyata, T. Ultra-long cycle fatigue of high-strength carbon steels part I: Review and analysis of the mechanism of failure. *Mater. Sci. Eng. A* **2003**, *356*, 227–235. [CrossRef]
14. Krewerth, D.; Lippmann, T.; Weidner, A.; Biermann, H. Influence of non-metallic inclusions on fatigue life in the very high cycle fatigue regime. *Int. J. Fatigue* **2016**, *84*, 40–52. [CrossRef]
15. Li, W.; Deng, H.; Liu, P. Interior Fracture Mechanism Analysis and Fatigue Life Prediction of Surface-Hardened Gear Steel under Axial Loading. *Materials* **2016**, *9*, 843. [CrossRef]
16. Torres, Y.; Rodríguez, S.; Mateo, A.; Anglada, M.; Llanes, L. Fatigue behavior of powder metallurgy high-speed steels: Fatigue limit prediction using a crack growth threshold-based approach. *Mater. Sci. Eng. A* **2004**, *387–389*, 501–504. [CrossRef]
17. Fernandez, A.; Pautler, S.E. Metal Fatigue—Effects of Small Defects and Nonmetallic Inclusions. *JSLS J. Soc. Laparoendosc. Surg.* **2011**, *15*, 421–423. [CrossRef] [PubMed]
18. Fukaura, K.; Yokoyama, Y.; Yokoi, D.; Tsujii, N.; Ono, K. Fatigue of cold-work tool steels: Effect of heat treatment and carbide morphology on fatigue crack formation, life, and fracture surface observations. *Metall. Mater. Trans. A* **2004**, *35*, 1289–1300. [CrossRef]
19. Verdiere, A.; Cerda, F.C.; Llanes, A.B.; Wu, J.; Crebolder, L.; Petrov, R. Effect of the austenitizing parameters on the microstructure and mechanical properties of 75Cr1 tool steel. *Mater. Sci. Eng. A* **2020**, *785*, 139331. [CrossRef]
20. Leskovšek, V.; Šuštaršič, B.; Jutriša, G. The influence of austenitizing and tempering temperature on the hardness and fracture toughness of hot-worked H11 tool steel. *J. Mater. Process. Technol.* **2006**, *178*, 328–334. [CrossRef]
21. Ali, M.; Porter, D.; Kömi, J.; Eissa, M.; El Faramawy, H.; Mattar, T. The effect of double austenitization and quenching on the microstructure and mechanical properties of CrNiMoWMnV ultrahigh-strength steels after low-temperature tempering. *Mater. Sci. Eng. A* **2019**, *763*, 138169. [CrossRef]

22. Patil, N.; Kakkeri, S. Sangamesh. Effect of Cryogenic Treated and Untreated Tool on its Tool Life-Review. *Int. J. Sci. Res.* **2014**, *3*, 141–145.
23. Pellizzari, M.; Molinari, A.; Gialanella, S.; Straffelini, G. Effect of deep cryogenic treatment on the microstructural properties of AISI H13 steel. *Metall. Ital.* **2001**, *93*, 21–27.
24. Sola, R.; Veronesi, P.; Giovanardi, R.; Forti, A.; Parigi, G. Effect of heat treatment before cryogenic cooling on the proprieties of AISI M2 steel. *Metall. Ital.* **2017**, *109*, 5–16.
25. Molinari, A.; Pellizzari, M.; Gialanella, S.; Straffelini, G.; Stiasny, K. Effect of deep cryogenic treatment on the mechanical properties of tool steels. *J. Mater. Process. Technol.* **2001**, *118*, 350–355. [CrossRef]
26. Pérez, M.; Belzunce, F.J. The effect of deep cryogenic treatments on the mechanical properties of an AISI H13 steel. *Mater. Sci. Eng. A* **2015**, *624*, 32–40. [CrossRef]
27. Sonar, T.; Lomte, S.; Gogte, C. Cryogenic Treatment of Metal—A Review. *Mater. Today: Proc.* **2018**, *5*, 25219–25228. [CrossRef]
28. Das, D.; Dutta, A.K.; Ray, K.K. Sub-zero treatments of AISI D2 steel: Part II. Wear behavior. *Mater. Sci. Eng. A* **2010**, *527*, 2194–2206. [CrossRef]
29. Das, D.; Sarkar, R.; Dutta, A.; Ray, K.K. Influence of sub-zero treatments on fracture toughness of AISI D2 steel. *Mater. Sci. Eng. A* **2010**, *528*, 589–603. [CrossRef]
30. Niaki, K.S.; Vahdat, S.E. Fatigue Scatter of 1.2542 Tool Steel after Deep Cryogenic Treatment. *Mater. Today: Proc.* **2015**, *2*, 1210–1215. [CrossRef]
31. Vahdat, S.E.; Nategh, S.; Mirdamadi, S. Microstructure and tensile properties of 45WCrV7 tool steel after deep cryogenic treatment. *Mater. Sci. Eng. A* **2013**, *585*, 444–454. [CrossRef]
32. Shinde, T.; Dhokey, N.B. Influence of Tertiary Carbides on Improving Fatigue Limit of H13 Die Steels. *Met. Microstruct. Anal.* **2017**, *6*, 398–406. [CrossRef]
33. Sola, R.; Giovanardi, R.; Parigi, G.; Veronesi, P. A Novel Methods for Fracture Toughness Evaluation of Tool Steels with Post-Tempering Cryogenic Treatment. *Metals* **2017**, *7*, 75. [CrossRef]
34. Collins, D.N. Deep Gryogenic Treatment of Tool Steels: A Review. *Heat Treat. Met.* **1996**, *2*, 40–42.
35. Pellizzari, M.; Molinari, A.; Girardini, L.; Maldarelli, L. Deep cryogenic treatment of AISI M2 high-speed steel. *Int. J. Microstruct. Mater. Prop.* **2008**, *3*, 383. [CrossRef]
36. Gonçalves, V.R.M.; Podgornik, B.; Leskovšek, V.; Totten, G.E.; Canale, L.D.C.F. Influence of Deep Cryogenic Treatment on the Mechanical Properties of Spring Steels. *J. Mater. Eng. Perform.* **2019**, *28*, 769–775. [CrossRef]
37. Available online: https://www.bohler-edelstahl.com/en/products/k890/ (accessed on 6 July 2021).
38. *ISO 14707:2021*; Surface Chemical Analysis—Glow Discharge Optical Emission Spectrometry (GD-OES)—Introduction to Use. International Organization for Standardization: Geneva, Switzerland, 2021.
39. *ASTM E3-11*; Standard Guide for Preparation of Metallographic Specimens. ASTM International: West Conshohocken, PA, USA, 2017.
40. *ASTM E407-07*; Standard Practice for Microetching Metals and Alloys. ASTM International: West Conshohocken, PA, USA, 2015.
41. *ASTM E975-13*; Standard Practice for X-ray Determination of Retained Austenite in Steel with Near Random Crystallo-Graphic Orientation. ASTM International: West Conshohocken, PA, USA, 2013.
42. *ISO 14577-1:2015*; Metallic Materials—Instrumented Indentation Test for Hardness and Materials Parameters—Part 1: Test Method. International Organization for Standardization: Geneva, Switzerland, 2015.
43. Sola, R.; Veronesi, P.; Giovanardi, R.; Parigi, G. A Novel Duplex Treatment of C20 Steel Combining Low-Pressure Carburizing and Laser Quenching. *J. Mater. Eng. Perform.* **2017**, *26*, 5396–5403. [CrossRef]
44. Sola, R.; Poli, G.; Veronesi, P.; Giovanardi, R. Effects of Surface Morphology on the Wear and Corrosion Resistance of Post-Treated Nitrided and Nitrocarburized 42CrMo4 Steel. *Met. Mater. Trans. A* **2014**, *45*, 2827–2833. [CrossRef]
45. *ISO 6507-1:2018*; Metallic materials—Vickers hardness test—Part 1: Test method. International Organization for Standardization: Geneva, Switzerland, 2018.
46. *ISO 6892-1:2019*; Metallic materials—Tensile testing—Part 1: Method of test at room temperature. International Organization for Standardization: Geneva, Switzerland, 2019.
47. *ISO 1143:2010*; Metallic Materials—Rotating bar Bending Fatigue Testing. International Organization for Standardization: Geneva, Switzerland, 2010.
48. Noda, N.-A.; Takase, Y. Stress concentration formula useful for all notch shape in a round bar (comparison between torsion, tension and bending). *Int. J. Fatigue* **2006**, *28*, 151–163. [CrossRef]
49. Young, W.C.; Budynas, R.G. *Roark's Formulas for Stress and Strain*, 7th ed.; McGraw Hill: New York, NY, USA, 2002.
50. *ISO 12107:2012*; Metallic Materials—Fatigue Testing—Statistical Planning and Analysis of Data. International Organization for Standardization: Geneva, Switzerland, 2012.
51. *DIN 4768*; Determination of values of surface roughness parameters Ra. Rz, Rmax using electrical contact (stylus) instruments Concepts and measuring conditions. Deutsches Institut für Normung e. V.: Berlin, Germany, 1990.
52. Totten, G.E. *Steel Heat Treatment*, 1st ed.; CRC Press: Boca Raton, FL, USA, 2006; ISBN 9780849384530.
53. Totten, G.E. Steel Heat Treating Fundamentals and Processes. In *ASM Handbook*; ASM International: Materials Park, Geauga County, OH, USA, 2013; Volume 4A.

54. Balijepalli, S.; Donnini, R.; Kaciulis, S.; Montanari, R.; Varone, A. Young's Modulus Profile in Kolsterized AISI 316L Steel. *Mater. Sci. Forum* **2013**, *762*, 183–188. [CrossRef]
55. Balijepalli, S.K.; Colantoni, I.; Donnini, R.; Kaciulis, S.; Lucci, M.; Montanari, R.; Ucciardello, N.; Varone, A. Modulo elastico della fase S in un acciaio 316 L kolsterizzato. *Metall. Ital.* **2013**, *1*, 42–47.
56. Mao, K.S.; Sun, C.; Huang, Y.; Shiau, C.-H.; Garner, F.A.; Freyer, P.D.; Wharry, J.P. Grain orientation dependence of nanoindentation and deformation-induced martensitic phase transformation in neutron irradiated AISI 304L stainless steel. *Materialia* **2019**, *5*, 100208. [CrossRef]
57. Yen, C.S.; Dolan, T.J. *A Critical Review of the Criteria for Notch-Sensitivity in Fatigue of Metals*; University of Illinois Bulletin: Urbana, OH, USA, 2007.
58. Kazymyrovych, V.; Bergström, J.; Burman, C. The Significance of Crack Initiation Stage in Very High Cycle Fatigue of Steels. *Steel Res. Int.* **2010**, *81*, 308–314. [CrossRef]
59. Murakami, Y. *Metal Fatigue: Effects of Small Defects and Non-Metallic Inclusions*; Elsevier: Amsterdam, The Netherlands, 2002.
60. Ghanem, F.; Braham, C.; Fitzpatrick, M.E.; Sidhom, H. Effect of Near-Surface Residual Stress and Microstructure Modification from Machining on the Fatigue Endurance of a Tool Steel. *J. Mater. Eng. Perform.* **2002**, *11*, 631–639. [CrossRef]
61. Shimatani, Y.; Shiozawa, K.; Nakada, T.; Yoshimoto, T.; Lu, L. The effect of the residual stresses generated by surface finishing methods on the very high cycle fatigue behavior of matrix HSS. *Int. J. Fatigue* **2011**, *33*, 122–131. [CrossRef]
62. Akiniwa, Y.; Miyamoto, N.; Tsuru, H.; Tanaka, K. Notch effect on fatigue strength reduction of bearing steel in the very high cycle regime. *Int. J. Fatigue* **2006**, *28*, 1555–1565. [CrossRef]
63. Das, D.; Dutta, A.; Ray, K. Correlation of microstructure with wear behaviour of deep cryogenically treated AISI D2 steel. *Wear* **2009**, *267*, 1371–1380. [CrossRef]
64. Çakir, F.H.; Çelik, O.N. The effects of cryogenic treatment on the toughness and tribological behaviors of eutectoid steel. *J. Mech. Sci. Technol.* **2017**, *31*, 3233–3239. [CrossRef]
65. Huang, J.; Zhu, Y.; Liao, X.; Beyerlein, I.; Bourke, M.; Mitchell, T. Microstructure of cryogenic treated M2 tool steel. *Mater. Sci. Eng. A* **2003**, *339*, 241–244. [CrossRef]
66. Gavriljuk, V.; Theisen, W.; Sirosh, V.; Polshin, E.; Kortmann, A.; Mogilny, G.; Petrov, Y.N.; Tarusin, Y.V. Low-temperature martensitic transformation in tool steels in relation to their deep cryogenic treatment. *Acta Mater.* **2013**, *61*, 1705–1715. [CrossRef]
67. Senthilkumar, D.; Rajendran, I.; Pellizzari, M.; Siiriainen, J. Influence of shallow and deep cryogenic treatment on the residual state of stress of 4140 steel. *J. Mater. Process. Technol.* **2011**, *211*, 396–401. [CrossRef]
68. Budynas, R.; Nisbett, K. *Shigley's Mechanical Engineering Design*, 10th ed.; McGraw-Hill: New York, NY, USA, 2015.
69. Kuhn, P.; Hardraht, H.F. *An Engineering Method for Estimating the Notch-Size Effect in Fatigue Test on Steel*; Technical Note (TN) 2805; National Advisory Committee for Aeronautics (NACA): Washington, DC, USA, 1952.
70. Hu, Z.-Z.; Cao, S.-Z. Relationship between fatigue notch factor and strength. *Eng. Fract. Mech.* **1994**, *48*, 127–136. [CrossRef]
71. Neuber, H. *Theory of Notch Stresses: Principles for Exact Calculation of Strength with Reference to Structural Form And material*; United States Atomic Energy Commission (USAEC) Office of Technical Services: Oak Ridge, TN, USA, 1961.
72. Peterson, R.E. *Stress Concentration Factors*; John Wiley: New York, NY, USA, 1974.
73. Heywood, R.B. *Designing against Fatigue*; Chapmann and Hall: London, UK, 1962.
74. Hu, Z.Z.; Cao, S.Z. Relation Between strain-hardening exponent and strength. *J. Wan Jiaotong Univ.* **1993**, *27*, 71–76.